



1 **Future tropospheric ozone budget and distribution over** 2 **East Asia under a Net Zero scenario**

3 Xuewei Hou¹, Oliver Wild², Bin Zhu¹, James Lee³

4 ¹Collaborative Innovation Center on Forecast and Evaluation of Meteorological Disasters, Key
5 Laboratory of Meteorological Disaster, Ministry of Education (KLME), School of Atmospheric
6 Physics, Nanjing University of Information Science and Technology, Nanjing, China

7 ²Lancaster Environment Centre, Lancaster University, Lancaster, UK

8 ³Department of Chemistry, University of York, York, UK

9 *Correspondence to:* Xuewei Hou (houxw@nuist.edu.cn)

10 **Abstract:** Under future net zero emission policies, reductions in emissions of ozone (O₃) precursors are
11 expected to alter the temporal and spatial distribution of tropospheric O₃. In this study, we quantify
12 changes in the tropospheric O₃ budget, spatiotemporal distribution of surface O₃ in East Asia and the
13 contributions from regional emissions, intercontinental transport and climate change between the present
14 day and 2060 under a net zero scenario, using the NCAR Community Earth System Model (CESM) with
15 online tagging of O₃ and its precursors. The results reveal that the global tropospheric O₃ burden is likely
16 to decrease by more than 20%, from 316 Tg in present day to 247 Tg in 2060, under a net zero scenario.
17 The burden of stratospheric O₃ in the troposphere is expected to increase from 69 to 77 Tg. The mean
18 lifetime of tropospheric O₃ increases by 2 days, ~10%. Changes in climate under a net zero pathway are
19 relatively small, and only lead to small increases in tropospheric O₃. Over East China, surface O₃
20 increases in winter, due to the weakened titration of O₃ by NO associated with reduced anthropogenic
21 NO emissions, and to enhanced stratospheric input. In summer, surface O₃ decreases by more than 30
22 ppbv, and peak concentrations shift from July to May. Local contributions from anthropogenic emissions
23 to surface O₃ over East Asia are highest in summer, but drop substantially, from 30% to 14%, under a
24 net zero scenario. The contribution of biogenic sources is enhanced, and forms the dominant contributor
25 to future surface O₃, especially in summer, ~40%. This enhanced contribution is mainly due to the
26 increased O₃ production efficiency under lower anthropogenic precursor emissions. Over Eastern China,
27 local anthropogenic contributions decrease from 50% to 30%. The decreases in surface O₃ are strongly
28 beneficial, and are more than sufficient to counteract the increases in surface O₃ observed in China over
29 recent years. This study thus highlights the important co-benefits of net zero policies that target climate
30 change in addressing surface O₃ pollution over East Asia.

31 **Keywords:** Tropospheric O₃; SSP1-1.9 pathway; net zero; O₃ budgets; stratospheric contribution

32 **1 Introduction**



33 Although ozone (O_3) occurs naturally in small quantities in the lower troposphere, unhealthy levels of
34 tropospheric O_3 are created when high levels of anthropogenic pollutants, such nitrogen oxides (NO_x),
35 and volatile organic compounds (VOCs) are oxidized in the presence of solar radiation. This excess O_3
36 acts as a pollutant and greenhouse gas, contributing to harmful smog that damages human health and
37 ecosystems (Jerrett et al., 2009; Malley et al., 2017; Emberson, 2020) and contributes to higher
38 temperatures near Earth's surface (Myhre et al., 2013; Stevenson et al., 2013). The relatively short
39 lifetime of O_3 in the troposphere (~3 weeks, Young et al., 2013) means that it is classified as a Near Term
40 Climate Forcer (NTCF), having an important influence on climate over shorter timescales. Tropospheric
41 O_3 also is an oxidant and a precursor for the hydroxyl (OH) radical (Griffiths et al., 2021). OH (and by
42 implication O_3) controls the lifetime of methane (Voulgarakis et al., 2013), the second most important
43 anthropogenic greenhouse gas after carbon dioxide (Myhre et al., 2013). Oxidant levels mediate the
44 formation of secondary aerosols such as sulfate and nitrate and play a major role in the aerosol budget
45 and burden with important consequences for radiative forcing (Shindell et al., 2009; Karset et al., 2018).
46 Understanding how tropospheric O_3 changes is important for both future air quality and climate (Turnock
47 et al., 2019).

48 A multi-model assessment of future changes in tropospheric O_3 was made in the Atmospheric Chemistry
49 and Climate Model Intercomparison Project (ACCMIP), using future changes in climate and O_3
50 precursor emissions from the Representative Concentration Pathways (RCPs) (Lamarque et al., 2013).
51 The models participating in ACCMIP projected changes in global annual mean surface O_3 concentrations
52 between 2000 and 2030 of ± 1.5 ppbv under the different RCPs (Young et al., 2013). More recent single
53 model estimates by O'Connor et al. (2014) and Kim et al. (2015) predict surface O_3 responses across the
54 different RCPs of between -4.0 and $+2.0$ ppbv by 2050 relative to 2000. The global annual mean
55 tropospheric O_3 burden was projected to change by between -18% and $+20\%$ from 2000 to 2100 under
56 the different RCPs (Cionni et al., 2011; Kawase et al., 2011; O'Connor et al., 2014; Young et al., 2013).
57 Whether tropospheric O_3 increases or decreases in future is dependent on the climate mitigation measures
58 that are taken. In preparation for the sixth Coupled Model Intercomparison Project (CMIP6), a new set
59 of future pathways were created. Five different socio-economic pathways (SSPs) were developed with
60 centennial trends based on different combinations of social, economic and environmental developments
61 (O'Neill et al., 2014). Different levels of emissions mitigation were included within each SSP to meet
62 particular climate and air pollution targets (Rao et al., 2017; Riahi et al., 2017). They incorporate stronger
63 links between socio-economic development patterns and climate change risks than previous assessments
64 and provide better hypothetical scenarios for future projections. The five most widely-used scenarios are
65 SSP1-1.9, SSP1-2.6, SSP2-4.5, SSP3-7.0, and SSP5-8.5, where SSP1-SSP5 represent differing
66 development storylines and the suffix 1.9~8.5 indicates the radiative forcing values (W/m^2) at the end of
67 the 21st century compared with those before the Industrial Revolution. These pathways provide a good
68 foundation for assessment of air quality, radiative forcing, ecological environmental effects and human
69 health effects in the future. Many studies have focused on the pessimistic SSP3-7.0 scenario reflecting
70 regional rivalry, and Griffiths et al. (2021) found that the tropospheric O_3 burden increases from
71 356 ± 31 Tg in present day to 416 ± 35 Tg in 2100 under this pathway. The sustainability-focused SSP1-
72 1.9 pathway is the scenario mostly closely aligned with recent pledges aiming at net zero greenhouse gas



73 emissions, limiting warming to 1.5°C by 2100, but the impacts of this pathway on tropospheric O₃ are
74 less well studied and remain unclear.

75 In East Asia, surface O₃ has increased rapidly since 2000 (Lu et al., 2020), and is expected to increase
76 by another ~10 ppbv by 2050 (Wang et al., 2013; Zhu and Liao, 2016; Hong et al., 2019). In September
77 2020, China committed to achieve carbon neutrality by 2060, following the commitments of many
78 developed countries to achieve net zero emissions by 2050. The effect of these strong mitigation
79 measures on surface O₃ has not been explored thoroughly, but the proposed emission pathway to net zero
80 loosely aligns with the SSP1-1.9 pathway. Turnock et al (2019) showed large reductions of >8 ppbv in
81 surface O₃ over East Asia by 2050 along this pathway due to large reductions in precursor emissions and
82 CH₄. The study also shows that any benefits to surface O₃ from reducing local emission sources over
83 East Asia could be offset by intercontinental transport of O₃ formed from sources remote to the region
84 and from global CH₄ sources. This analysis used an O₃ parameterization to rapidly assess changes in O₃
85 and source attribution (Wild et al., 2012; Turnock et al., 2018), but did not account for changes in climate,
86 stratosphere-to-troposphere exchange, or chemical regime. Wang and Liao (2022) found that the annual
87 mean contribution of Southeast Asia to surface MDA8 O₃ in China is 3-19 µg m⁻³, about 2-10 ppbv, and
88 this contribution is reduced in future along the SSP1-1.9 pathway. However, this study used fixed
89 meteorological parameters for 2015, preventing quantification of regional transport contributions and
90 stratosphere-tropospheric exchange. Other recent assessments exploring the implications of carbon
91 neutrality in China have suggested that there may be reductions in MDA8 O₃ of more than 30 µg m⁻³ (15
92 ppb) by 2060 and that regional mean O₃ concentrations may decline to 63.0 µg m⁻³ (Shi et al., 2021;
93 Wang and Liao, 2022; Xu et al., 2022).

94 While previous studies have quantified possible changes in surface O₃ under carbon neutrality, the wider
95 impact on the global tropospheric O₃ budget and the changing contributions of different sources remain
96 unclear. In this study, we quantify the changes in surface O₃ over East Asia, and especially over Eastern
97 China which currently has high anthropogenic emissions, and the contribution of different sources based
98 on emissions and climate change along the SSP1-1.9 pathway, using the NCAR Community Earth
99 System Model (CESM) with online tagging of O₃ and its precursors. We present a self-consistent
100 assessment of the changes in surface O₃ associated with changes in emissions and climate, along with
101 the first attribution of these changes. The paper is organized as follows. Section 2 describes the model
102 configurations, experimental settings, O₃ tagging method, and evaluation datasets. In section 3, O₃ and
103 NO_x in present day simulations is evaluated against observations. In section 4, changes in tropospheric
104 O₃ under the net zero scenario are presented. In section 5, the contribution of O₃ chemistry and
105 intercontinental transport are discussed under present day and future conditions. We close with a
106 summary in section 6.

107 **2 Materials and methods**

108 **2.1 Model configurations and experiments**



109 The NCAR Community Earth System Model (CESM) is a coupled climate model incorporating
110 components for simulating the Earth's atmosphere, ocean, land, land-ice, and sea-ice (e.g., Neale et al.,
111 2013; Lamarque et al., 2012; Tilmes et al., 2015; Danabasoglu et al., 2020), allowing fundamental
112 research into the Earth's past, present, and future climate states. The experiments here use CESM version
113 1.2.2 (<https://www.cesm.ucar.edu/models/cesm1.2/>) and the latest version 2.2.0
114 (<https://www.cesm.ucar.edu/models/cesm2/>), to reproduce present-day O₃ mixing ratios and to predict
115 O₃ responses to emissions and climate in the future along the SSP1-1.9 pathway. All model simulations
116 are performed with prescribed sea surface temperatures and sea ice distribution data for climatological
117 conditions in present day and future net zero, since we focus on the atmospheric component. Dry
118 deposition of gases and aerosols are implemented in the Community Land Model (Oleson, 2010) as
119 described in Lamarque et al. (2012).

120 Atmospheric chemistry of gas phase and aerosol species in the global Community Atmosphere Model
121 (CAM version 4, Neale et al., 2013; CAM version 6, Danabasoglu et al., 2020), the atmospheric
122 component of the Community Earth System Model (CESM), is represented by CAM-chem. CAM-chem
123 provides the flexibility of using the same code to perform climate simulations (online) and simulations
124 with specified meteorological fields (offline). The chemical mechanism is based on the Model for Ozone
125 and Related chemical Tracers (MOZART), version 4 mechanism for the troposphere (Emmons et al.,
126 2010), extended for stratospheric chemistry (Kinnison et al., 2007), with further updates as described in
127 Lamarque et al. (2012), including additional reaction rate updates following JPL-2010 recommendations
128 (Sander et al., 2011).

129 In this paper, offline simulations are used to investigate the effect of emission changes on tropospheric
130 O₃ under fixed meteorological parameters, while online simulations are used for the effects of emission
131 and climate changes with two-way feedback of atmospheric components and meteorological parameters.
132 Two different versions of CESM are used in this study due to the application of online tagging of O₃ and
133 its precursors, which is only fully tested and evaluated in CESM1. All simulations discussed in this paper
134 are performed at a horizontal resolution of 1.9° (latitude) and 2.5° (longitude). The model has 26 vertical
135 levels in the online configuration and 56 levels in the offline configuration using specified meteorological
136 fields; in all these cases, the model extends to approximately 4 hPa (≈40 km). Offline simulations were
137 driven by Modern Era Retrospective analysis for Research and Applications (MERRA2) meteorology
138 (Rienecker et al., 2011). Simulations using present-day emissions (2015) are labelled PD, while those
139 using future net zero emissions (2060) are labelled NZ, and these are prefixed with online or offline
140 depending whether the model is run online or driven by MERRA2 meteorology. To ensure the stability
141 of the response to climate change, the future online simulations are run for 15 years, with the first ten
142 years as spin-up. The CH₄ concentrations are prescribed following the SSP1-1.9 pathway using a fixed
143 lower boundary condition. A summary of the simulations is provided in Table 1.

144

Table 1 Experimental settings

| Case-name | Climate Change and Emissions | Emissions |
|-----------|------------------------------|-----------|
|-----------|------------------------------|-----------|



| | online-PD | online-NZ | offline-PD | offline-NZ |
|--------------------------------|---|--------------------------|--|--------------------------|
| Model | CESM1.2.2 | CESM1.2.2 | CESM2.2.0 | CESM2.2.0 |
| Component | FMOZ | FMOZ | FCSD | FCSD |
| Physics | CAM4 | CAM4 | CAM6 | CAM6 |
| Chemical mechanism | tropospheric chemistry with bulk aerosols, MOZART-4 | | troposphere/stratosphere chemistry with simplified VBS-SOA, MOZART-TS1 | |
| Dynamics | Free-running | Free-running | Merra2 Nudging | Merra2 Nudging |
| Spin-up | 2012-2014 | 2050-2059 | 2014 | 2014 |
| Analyzed Year | 2015-2016 | 2060-2064 | 2015 | 2015 |
| Resolution | 1.9°×2.5° with 26 levels | 1.9°×2.5° with 26 levels | 1.9°×2.5° with 56 levels | 1.9°×2.5° with 56 levels |
| in China | 2015- DPEC | 2060-DPEC | 2015-CMIP6 | 2060-DPEC |
| Emission Outside China | 2015-SSP119 | 2060-SSP119 | 2015-CMIP6 | 2060-SSP119 |
| CH ₄ | 2015-SSP119 | 2060-SSP119 | 2015-SSP119 | 2060-SSP119 |
| Tagging O ₃ sources | TOAST | | O3S | |

145

146 **2.2 Emissions**

147 For this analysis, we use estimates of global future anthropogenic and biomass burning emissions and
 148 future abundances of greenhouse gases and aerosols provided by the SSP1-1.9 pathway ([https://esgf-](https://esgf-node.llnl.gov/projects/input4mips/)
 149 [node.llnl.gov/projects/input4mips/](https://esgf-node.llnl.gov/projects/input4mips/)) along with more recent estimates for China using the Ambitious-
 150 pollution-Neutral-goals scenario from the Dynamic Projection model for Emissions in China (DPEC,
 151 <http://meicmodel.org/>). The SSP1-1.9 pathway results in a climate radiative forcing of 1.9 W m⁻² by 2100
 152 under the sustainable development path. The SSP1-1.9 pathway is a strong pollution control scenario and
 153 is the only route to limit the global average temperature increase since the preindustrial period to 1.5°C
 154 by 2100 (O'Neill et al., 2014; Rao et al., 2017; Riahi et al., 2017). The emissions inventory includes
 155 monthly O₃ precursors, aerosols, and their precursors (NO_x, CO, non-methane volatile organic (VOCs),
 156 sulfur dioxide (SO₂), ammonia (NH₃), black carbon (BC), organic carbon (OC), dimethyl sulphide
 157 (DMS)), and concentrations of greenhouse gases, such as CH₄. Biogenic emissions of VOCs are
 158 calculated online in CESM using the Model of Emissions of Gases and Aerosols from Nature model
 159 (MEGAN; Guenther et al., 2006; 2012). We use emissions for the years 2015 and 2060. Over China, the
 160 anthropogenic emissions are replaced by the Ambitious-pollution-Neutral- goals scenario from DPEC
 161 (Tong et al., 2020; Cheng et al., 2021). This considers a scenario in which China achieves carbon
 162 neutrality by 2060. The combined emissions distribution for NO_x and its changes in future are shown in
 163 Figure S1. The total annual mean surface emissions of key pollutants from anthropogenic (ANT),



164 biomass burning (BB) and biogenic (BIO) sources for the present day (2015) and future net zero (2060)
 165 over the globe and in East Asia are listed in Table 2.

166 The global anthropogenic emissions of all O₃ precursors are significantly reduced in the net zero scenario.
 167 Due to strict control policies on pollutants emissions and changes in technology and behavior, global
 168 anthropogenic NO emissions decrease from 87 Tg yr⁻¹ in present day to 19 Tg yr⁻¹ in 2060, and total
 169 anthropogenic VOCs emissions decrease from 125 Tg yr⁻¹ to 28 Tg yr⁻¹. Biomass burning emissions
 170 decrease slightly. Natural NO soil emission, VOCs biogenic emission, and CO ocean emission are
 171 assumed not to change in this study as changes in land use are relatively small. Anthropogenic emissions
 172 over East Asia account for more than 35% of the global total, with biomass combustion emissions
 173 accounting for a smaller proportion, ~10%, and natural emissions of NO, VOCs and CO accounting for
 174 ~20%. The decrease of anthropogenic emissions over East Asia (about 80% for NO) is greater than the
 175 global average, >70%, which may due to the high present day emissions over the region, especially in
 176 Eastern China. The global CH₄ concentration decreases from the current 1831 ppbv to 1312 ppbv, due
 177 to the lower global CH₄ emissions under net zero.

178 Table 2 Annual mean time-varying surface emissions of NO_x, VOCs, CO, sulfur dioxide (SO₂), black
 179 carbon (BC), and organic carbon (OC) from anthropogenic (ANT), biomass burning (BB) and biogenic
 180 (BIO) emissions for the present day (2015) and future (2060, net zero) in East Asia and over globe.

181 Annual mean surface CH₄ mixing ratios (ppbv) are also shown.

| Emission (Tg yr ⁻¹) | | Globe | | East Asia | |
|---------------------------------|-------|-------------|----------|-------------|----------|
| | | Present Day | Net Zero | Present Day | Net Zero |
| NO | ANT | 87.5 | 19.1 | 36.9 | 7.5 |
| | BB | 8.9 | 7.5 | 0.7 | 0.5 |
| | Soil | 10.6 | 10.6 | 2.3 | 2.3 |
| | Total | 106.9 | 37.2 | 39.8 | 10.2 |
| VOCs | ANT | 125.0 | 27.5 | 42.9 | 11.0 |
| | BB | 66.6 | 50.2 | 6.3 | 4.0 |
| | BIO | 868.5 | 868.5 | 111.0 | 111.0 |
| | Total | 1060.1 | 946.2 | 160.3 | 126.0 |
| CO | ANT | 559.8 | 151.7 | 266.9 | 72.7 |
| | BB | 325.5 | 248.2 | 30.2 | 18.9 |
| | Ocean | 20.0 | 20.0 | 1.3 | 1.3 |
| | Total | 905.2 | 419.9 | 298.4 | 92.9 |
| SO ₂ | ANT | 105.2 | 18.8 | 40.2 | 4.8 |
| | BB | 2.1 | 1.7 | 0.2 | 0.1 |



| | | | | | |
|------------------------|-------|--------|--------|--------|--------|
| | Total | 107.4 | 20.5 | 40.4 | 5.0 |
| BC | ANT | 6.7 | 1.0 | 3.0 | 0.3 |
| | BB | 1.7 | 1.4 | 0.2 | 0.1 |
| | Total | 8.4 | 2.3 | 3.1 | 0.4 |
| OC | ANT | 16.5 | 4.1 | 6.5 | 1.4 |
| | BB | 15.1 | 10.6 | 1.6 | 0.9 |
| | Total | 31.5 | 14.8 | 8.1 | 2.3 |
| CH ₄ (ppbv) | | 1830.5 | 1312.2 | 1860.8 | 1337.3 |

182

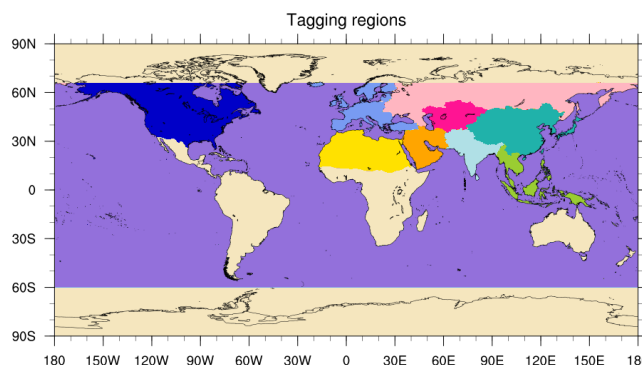
183 **2.3 Tagging of ozone**

184 In this study, we used the Tropospheric Ozone Attribution of Sources with Tagging (TOAST) ozone
 185 methodology in CESM1.2.2 previously described by Butler et al. (2018, 2020) to perform separate source
 186 attributions of ground-level O₃ to NO_x. The parameterizations based on the work of Butler et al. (2018,
 187 2020) include tagging biogenic, biomass burning and anthropogenic emissions of NO_x or VOCs by their
 188 geographical source regions. This tagging methodology allows us to examine the seasonal cycle of the
 189 surface O₃ attribution in receptor regions using those defined in the Hemispheric Transport of Air
 190 Pollutants Phase 2 (HTAP2, Janssens-Maenhout et al., 2015; Koffi et al., 2016). We considered 16
 191 sources, including 11 geographical source regions for anthropogenic NO_x, shown in Table 3 and Figure
 192 1, NO_x emissions from biogenic sources (BIO), biomass burning (BB), aircraft (AIR) and lightning
 193 (LIG), and O₃ originating in the stratosphere (STR).

194 Table 3 Source sector tagging of anthropogenic NO_x emissions by geographical source region, NO_x
 195 emissions from biogenic burning, soil emission, aircraft, and lightning, and the contribution of
 196 stratospheric O₃ input.

| ID | Geographical region, NO _x | ID | Geographical region, NO _x | ID | Source |
|-----|--------------------------------------|-----|--------------------------------------|-----|------------------------------|
| OCN | Oceans | NAF | Northern Africa | BIO | Biogenic NO _x |
| NAM | N. America | MDE | Middle East | BB | Bioburn NO _x |
| EUR | Europe | CAS | Central Asia | AIR | Aircraft NO _x |
| SAS | South Asia | SEA | South East Asia | LIG | Lightning NO _x |
| EAS | East Asia | RBU | Russia, Belarus, Ukraine | STR | Stratospheric O ₃ |
| RST | Rest of World | | | | |

197



198

199 Figure 1 Geographical source regions for tagging anthropogenic NO_x emissions in this study as defined
200 in HTAP Phase 2.

201 2.4 Measurement Data

202 To evaluate tropospheric column O₃ in the model simulations, we used a present-day satellite dataset of
203 tropospheric column O₃, which was derived by combining retrievals from the Aura Ozone Monitoring
204 Instrument (OMI) and Microwave Limb Sounder (MLS) observations ([https://acd-
205 ext.gsfc.nasa.gov/Data_services/cloud_slice/](https://acd-ext.gsfc.nasa.gov/Data_services/cloud_slice/)). More details about the generation of this dataset are
206 provided by Ziemke et al., (2011). The dataset resolution used in this study is 1° (Latitude) × 1.25°
207 (Longitude) and the year is 2015. The monthly-mean thermal tropopause pressure was used to separate
208 tropospheric and stratospheric O₃ for the model results and satellite observations.

209 A High-resolution Air Quality Reanalysis Dataset over China (CAQRA, Kong, et al., 2020; Tang et al.,
210 2020 a, b) was used to evaluate the simulated present day surface O₃ over China
211 (<https://doi.org/10.11922/sciencedb.00053>). This dataset was generated by assimilating surface
212 observations from the China National Environmental Monitoring Centre (CNEMC) into the Nested Air
213 Quality Prediction Modeling System (Tang et al., 2011, Wang et al., 2000), and it provides self-consistent
214 concentration fields of O₃ in China from 2013 to 2019 at high spatial (15 km) and temporal (1 h)
215 resolutions. The year used in this study is 2015.

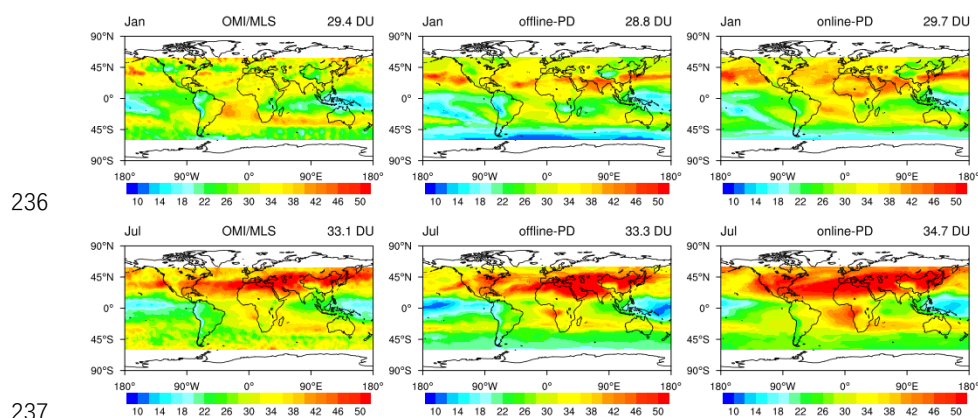
216 In addition, monthly observational surface O₃ concentration were taken from 12 regional stations of the
217 Acid Deposition Monitoring Network in East Asia (EANET; <https://www.eanet.asia/>) for 2015: Rishiri,
218 Ochiishi, Tappi, Sado-Seki, Happo, Oki, Yusuvara, Hedo, Mondy, Listvyanka, Kanghawa, and Chenju.
219 The locations and altitudes of these sites are shown in Figure S2.

220 3. Tropospheric ozone evaluation

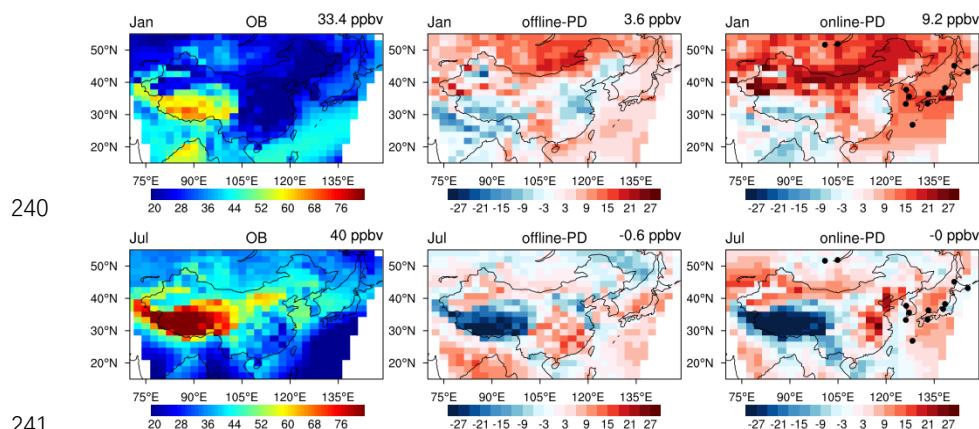
221 We compared the simulated monthly mean tropospheric column O₃ (TCO) with that derived from
222 OMI/MLS for January and July in 2015 (Figure 2). The model captures the general features of the
223 observed tropospheric column, reproducing the seasonal pattern, with a minimum of 15 DU at 180°E in
224 the tropics during January and a maximum of >50 DU in northern hemisphere mid-latitudes during July.



225 The highest values in the northern mid-latitudes are overestimated in both offline and online simulations,
 226 especially during July. In the simulations, TCO was calculated by integrating the O₃ from the surface to
 227 the tropopause. Some of the differences of the simulated TCO with OMI/MLS may be due to the
 228 relatively coarse vertical resolution of the model, which is averages 183 hPa for the online model near
 229 the tropopause (194 hPa in NCEP reanalysis datasets). Uncertainty in the satellite dataset (exceeding
 230 5DU in high latitudes, Ziemke et al. 2011) might also contribute to these differences. The global
 231 (60°S~60°N) annual mean tropospheric O₃ columns from the offline and online simulations are 31.3 and
 232 32.2 DU, respectively, which match those from OMI/MLS (31.6 DU) and the ACCMIP models mean
 233 value (30.8 DU, Young et al., 2013) well. The online simulated tropospheric ozone column on global
 234 annual average is the highest, due to the coarser vertical resolution in online simulation (Lamarque et al.,
 235 2012).



236
 237
 238 Figure 2 Tropospheric column O₃ (DU) from OMI/MLS (left), offline (middle) and online (right)
 239 simulations for January and July under present day conditions.



240
 241
 242 Figure 3 Surface O₃ mixing ratios in East Asia (ppbv) from the CAQRA reanalysis (left) and the biases
 243 from offline (middle) and online (right) present day simulations in January and July. The biases are



244 simulations minus observations, and black dots show the locations of EANET observation sites. The
245 values in the right corner of each sub-figure are the regional mean for East Asia (15~55°N, 70~149°E).

246 As shown in Figure 3, surface O₃ shows substantial seasonal variations with low concentrations in winter
247 and high concentrations in summer. The spatial distributions of simulated surface O₃ concentrations
248 match the observations well. The online simulated surface O₃ (ppbv) is overestimated by 9.2 ppbv on
249 average in winter, especially in Mongolia, north and middle of China, Korea, and Japan, while the offline
250 simulation is much closer to the observation with a bias of 3.6 ppbv. The comparison of simulated surface
251 O₃ (ppbv) with EANET observations show that the simulations reproduce the seasonal variations at these
252 12 sites (Figure S2 in the Supplementary Material). In general, the performance of these simulations is
253 very similar to those from other chemical model studies (Li et al., 2019; Young et al., 2018).

254 **4 Tropospheric ozone budgets and distributions under the Net Zero scenario**

255 An overview of the global model diagnostics for the simulation experiments is given in Table 4.
256 Tropospheric O₃ burden and budget terms for present-day conditions in this study match previous results
257 well. Under net zero, the chemical production decreases from 5038 to 3392 Tg(O₃) yr⁻¹, and the chemical
258 loss decreases from 4641 to 3311 Tg(O₃) yr⁻¹. The net chemical tendency of tropospheric O₃ (NetChem
259 in Table 4) drops substantially, decreasing from the current 397 Tg(O₃) yr⁻¹ to 81 Tg(O₃) yr⁻¹, due to the
260 large reduction in O₃ precursor emissions (Table 2). This results in an increase in the lifetime of
261 tropospheric O₃ from 20 days to 22 days. The residual term, which principally reflects net transport from
262 the stratosphere, increases from the current 595 to 626 Tg(O₃) yr⁻¹. The global tropospheric O₃ burden
263 decreases by about 20%, from 316 Tg to 247 Tg, bringing it close to the mean burden of 239±22 Tg
264 estimated for the pre-industrial period (Young et al., 2013). The burden of O₃ of stratospheric origin in
265 the troposphere (O₃S) increases from 69 Tg to 77 Tg. This increased stratospheric contribution may be
266 due to the enhancement of stratospheric circulation and increased stratosphere-troposphere exchange
267 caused by climate change (Sudo et al., 2003; Lu et al., 2019). In addition, the longer chemical lifetime
268 allows stratospheric O₃ to persist for longer in the troposphere, enhancing the stratospheric contribution.

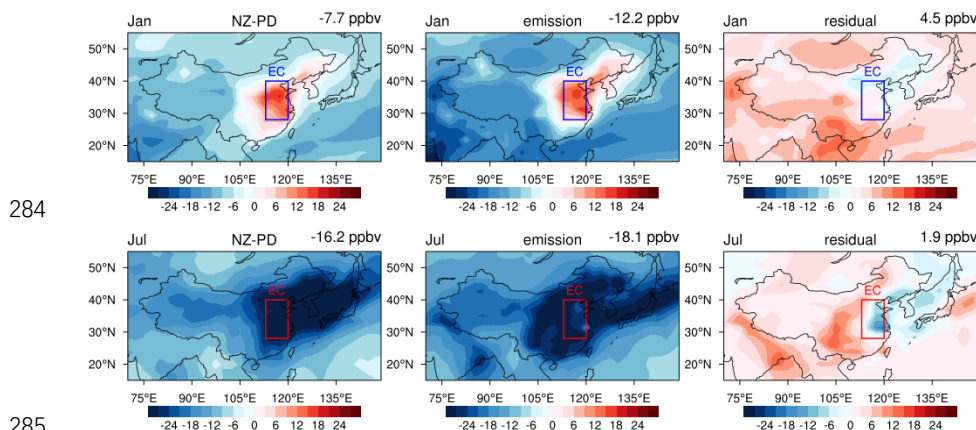
269 Over East Asia, the net photochemical production of tropospheric O₃ also decreases significantly, from
270 the current 227 Tg(O₃) yr⁻¹ to 137 Tg(O₃) yr⁻¹ under net zero, but the reduction is less than the global
271 average. The negative “Residual” budget term for East Asia indicates that East Asia is a net outflow
272 region for tropospheric O₃, and this outflow is weakened in the future, from 89 Tg(O₃) yr⁻¹ under present
273 day conditions to 38 Tg(O₃) yr⁻¹ under net zero, reflecting the reduced regional production. The
274 tropospheric O₃ burden in East Asia decreases from 25 Tg to 19 Tg, while the burden of O₃ from the
275 stratosphere increases slightly from 5 Tg to 6 Tg. The tropospheric O₃ lifetime in East Asia is 15 days,
276 slightly lower than the global average due to the faster photochemical processing under relatively high
277 anthropogenic emissions. But the increase of ~2 days matches that of the global average.



278 Table 4 Global tropospheric O₃ burden (Tg) and budget terms (Tg yr⁻¹) in chemical transport models.

| Models | Prod | Loss | NetChem | Residual | DryDep | Burden (O ₃ /O ₃ S) | Lifetime (days) | Reference |
|------------------|-------------|-------------|------------|------------------|------------|--|--------------------|-------------------------|
| Globe | | | | STE | | | | |
| 33 | 3948±761 | 3745±554 | 245±346 | 636±273 | 902±255 | 307±38 | 21-25 | Wild (2007) |
| 17 | 4465±514 | 4114±409 | 396±247 | 529±105 | 949±222 | 314±33 | 22±2 | Stevenson et al. (2006) |
| 15 | 5110±606 | 4668±727 | 442±309 | 552±168 | 1003±200 | 344±39 | 22±2 | Young et al. (2013) |
| PD | 5038 | 4641 | 397 | 595 | 992 | 316/69 | 20 | This study |
| NZ | 3392 | 3311 | 81 | 626 | 707 | 247/77 | 22 | This study |
| East Asia | | | | Transport | | | | |
| PD | 682 | 455 | 227 | -89 | 138 | 25/5 | 15 | This study |
| NZ | 430 | 293 | 137 | -38 | 99 | 19/6 | 17 | This study |

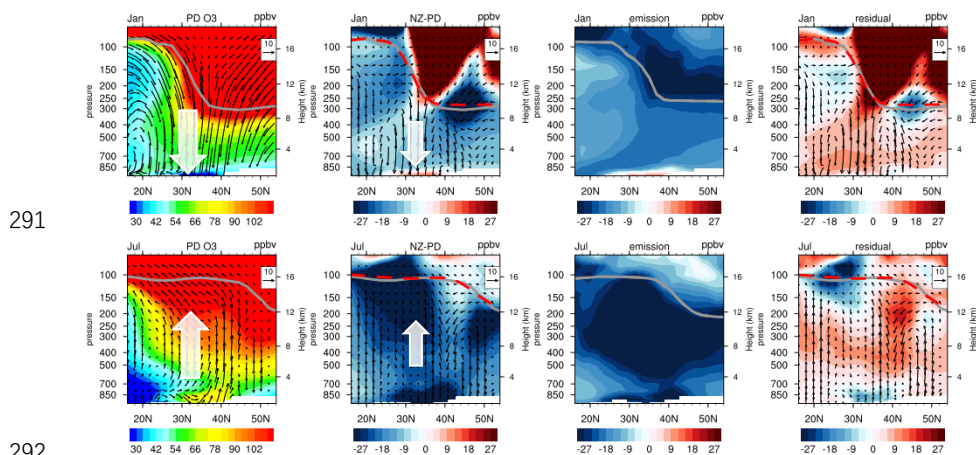
279 Prod for chemical production, Loss for chemical loss, Prod-Loss for net chemical production (NetChem)
 280 and DryDep for dry deposition; Residual is the term balance by Residual=Loss-Prod+DryDep. Units of
 281 Prod, Loss, NetChem, Residual and DryDep are in Tg(O₃) yr⁻¹, Burden in Tg(O₃), and Lifetime in days.
 282 The climatological pressure tropopause is used. PD is the online present day experiment simulation. NZ
 283 is online net zero experiment simulation.



284

285

286 Figure 4 Changes in surface O₃ mixing ratio (ppbv) over China in January and July between present
 287 day and net zero (online-NZ minus online-PD, left), and changes due to emissions (offline-NZ minus
 288 offline-PD, middle) and the residual (left minus middle panel, right). The values in the right corner of
 289 each panel are the regions mean over East Asia (15°~55°N, 70°~149°E). The frame is the region of
 290 Eastern China (EC, 28°~40°N, 113°~120°E).



291

292

293 Figure 5 Zonal mean O₃ cross section (ppbv) and wind speed (vectors, $v: m s^{-1}$, $w: (-500) pa s^{-1}$) over
 294 Eastern China (longitudes 111-122°E) in January and July under present day (online-PD, left), the
 295 changes in O₃ and wind speed (second panels) and changes due to emissions (third panels) and the
 296 residual (second panels minus third panels, right). Grey lines show the tropopause location under
 297 present day conditions; the red dashed lines show the tropopause location under net zero.

298 The changes in surface O₃ over East Asia between 2015 and 2060 in winter and summer are shown in
 299 Figure 4. The left panels show the changes in surface O₃ under net zero (online-NZ minus online-PD),
 300 which include the effects of climate change and emissions changes. The middle panels show the changes
 301 in surface O₃ under the effect of emissions changes only (offline-NZ minus offline-PD). The right panels



302 show the residual changes in surface O_3 which reflect the effect of climate change, but are also influenced
303 by differences in model setup between the online and offline simulations (left panels minus middle
304 panels). Surface O_3 decreases in East Asia under net zero, with a mean reduction of 7.7 ppbv in winter
305 and a greater reduction of 16.2 ppbv in summer. Turnock et al. (2019) estimated an annual mean
306 reduction of 8 ppbv in 2050 along the SSP1-1.9 pathway, slightly less than we find here. However, we
307 have used the more stringent DPEC Ambitious-pollution-Neutral-goals emission scenario for China
308 rather than the standard SSP1-1.9 pathway and we note that anthropogenic NO emissions in China are 2
309 $Tg(NO) yr^{-1}$ lower in this scenario than those in SSP1-1.9. Surface O_3 over Eastern China and South
310 Korea increases in winter in these scenarios, driven by the reduction in emissions (left and middle panels).
311 This increase in surface O_3 is caused by a weakening of titration under lower regional NO emissions. The
312 influence of climate change on surface O_3 is relatively weak, and leads to an increase of surface O_3 in
313 most parts of East Asia (right panels). This is partly due to enhanced vertical circulation leading to an
314 increased contribution from stratospheric O_3 (Akritidis et al., 2019; shown in Figure S3). Xu et al. (2022)
315 also showed that emission reduction is far more effective than climate change in improving air quality
316 ($PM_{2.5}$ and O_3) over East Asia under a carbon neutral reduction pathway. Here we will use tagging
317 simulations to quantify the contributions of different sources to surface O_3 changes over East Asia,
318 especially over Eastern China where surface O_3 increases in winter and decreases in summer.

319 It can be seen from the vertical distribution of O_3 and circulation (shown in the first panels of Figure 5)
320 that the O_3 concentration increases with altitude under present day conditions. At the same altitude, the
321 O_3 concentration is higher in middle and high latitudes than in low latitude. In winter, there is strong net
322 descent of air over eastern China (30~40°N), which weakens in spring, and turns to updraft in summer.
323 These may be due to the weakened Brewer-Dobson circulation and strengthened convection (Butchart,
324 2014; Wild and Akimoto, 2001). As shown in the second panels of Figure 5, there is a net decrease in
325 tropospheric O_3 in future, with an increase only seen near 30°N very close to the surface. In summer, the
326 reduction in tropospheric O_3 is greatest, especially near the tropopause where it exceeds 30 ppbv. In
327 addition, due to the temperature increase and circulation enhancement in the future, the tropopause height
328 increases, especially in the mid-latitude region in winter where the increase is about 7 hPa. As seen from
329 the third panels of Figure 5, the reduction of emissions from aircraft (NO emissions in Figure S1) leads
330 to a reduction in O_3 production, and the O_3 concentration near the tropopause decreases substantially in
331 the future. However, other factors such as climate change (the fourth panels in Figure 5) lead to increases
332 in tropospheric O_3 by 2060.

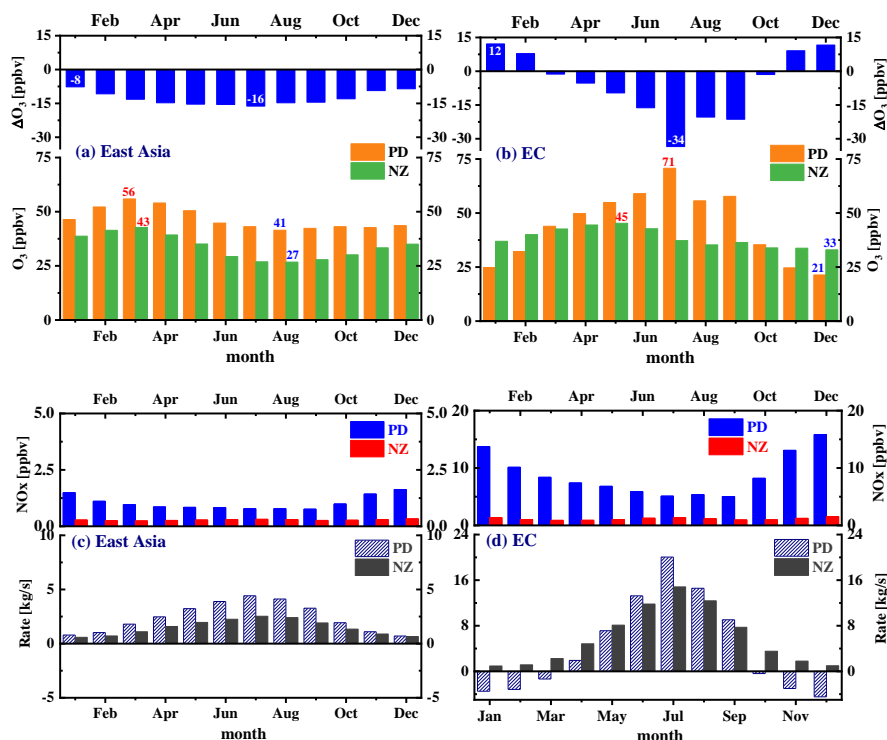
333 **5 The contribution of O_3 chemistry and intercontinental transport**

334 Surface O_3 shows substantial seasonal variation over East Asia with a peak in spring, as shown in Figure
335 6a. It reaches a maximum (56 ppbv) in March and is lowest (41 ppbv) in August under present day
336 conditions. Under net zero, the concentration of surface O_3 is lower throughout the year, and while the
337 peak is still in March, the mixing ratio drops to 43 ppbv. The decrease is greatest in July, 16 ppbv, which
338 reflects weaker chemical production in summertime under lower future emissions (Figure 6c). In contrast,
339 surface O_3 over Eastern China is highest (71 ppbv) in July and lowest (21 ppbv) in December under
340 present day conditions (Figure 6b). Under net zero, surface O_3 increases in winter and decreases in
341 summer, and the peak shifts from July to May, due to the changes in O_3 precursors emissions (Bowman
342 et al., 2021). The decrease is highest in July, as seen over the wider East Asian region, but is twice as



343 large, at 34 ppbv, reflecting the stronger present-day emissions over Eastern China. There is a substantial
 344 increase in O₃ in January of 12 ppbv, reflecting reduced titration by NO. The concentration of surface
 345 NO_x decreases more than 60%, and by an even larger factor in winter (~90%, 14 ppbv); and its seasonal
 346 variation is reduced which accounts for the reduction in anthropogenic emissions (Figure 6d). In terms
 347 of the O₃ chemical budget, local chemical production and destruction are both reduced in the future. The
 348 peak in net O₃ chemical production still occurs in summer which highlights that photochemical processes
 349 continue to dominate the seasonal variation of surface O₃ in Eastern China in future. However, the net
 350 chemical destruction that currently occurs in winter is replaced with a small net O₃ production (Figure
 351 6d), reflecting the reduced titration of O₃ by NO under future emissions, which are very greatly reduced
 352 under net zero.

353



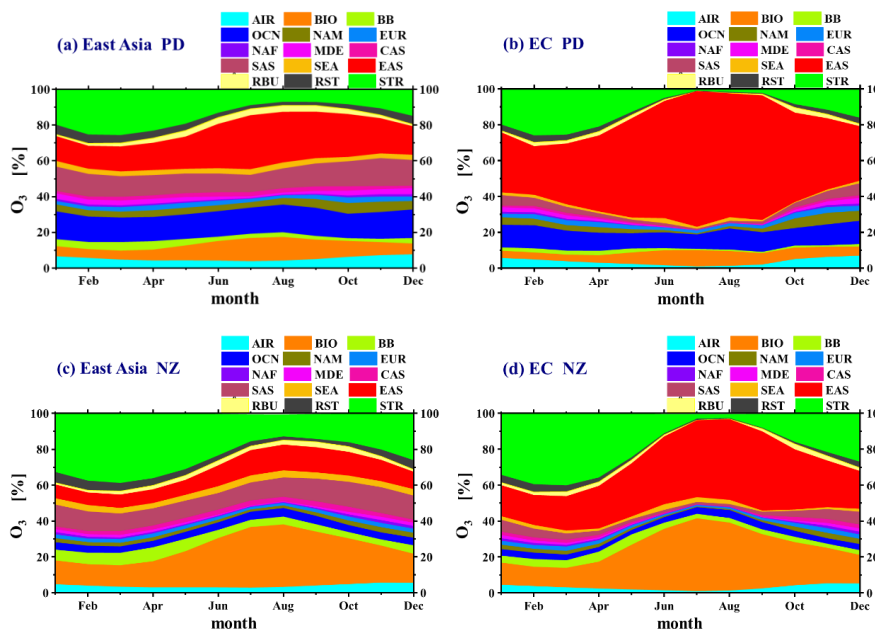
354

355 Figure 6 Comparison of O₃ (a, b), NO_x and net O₃ chemical tendency (c, d) at the surface under present
 356 day and net zero conditions over East Asia (left) and Eastern China (right). Results are from the online
 357 simulations (online-PD and online-NZ). Maximum and minimum O₃ mixing ratios are highlighted in
 358 red and blue, respectively, and the largest and smallest O₃ changes are indicated in white.

359 We quantify the contributions of regional transport and stratospheric input to surface O₃ on a monthly
 360 basis in Figure 7. We find that the contribution of anthropogenic NO emissions from East Asia (EAS) is
 361 highest, especially in summer when it reaches 30%. The contribution from biogenic NO emissions (BIO)
 362 is also important, exceeding 10% in summer. The contributions from the ocean (OCN) and from



363 anthropogenic NO emissions over South Asia (SAS) show little seasonal variation, both contributing 10-
 364 15%. Under net zero (Figure 7c), the contribution from East Asia drops dramatically, to 14% in summer,
 365 due to the reduced emissions of O₃ precursors. The contribution of biogenic sources is enhanced, and
 366 forms the dominant contributor to surface O₃ under net zero, especially in summer, ~40%. The emissions
 367 from biogenic sources are changed slightly in this study. The enhanced contribution of biogenic sources
 368 is mainly due to the increased O₃ production efficiency, which is a consequence of lower O₃ precursor
 369 concentrations (Kleinman et al., 2002; Zaveri et al., 2003). The contribution of oceanic sources decreases
 370 to 4% due to reduced emissions from shipping. The contribution from stratospheric O₃ (STR) is highest
 371 in March (26%, 14 ppbv), lowest in August (7%, 3 ppbv) under present day conditions. Under net zero,
 372 the highest contribution is increased to 39% (17 ppbv), and the lowest contribution is also increased, to
 373 12% (3 ppbv). This may due to enhanced stratospheric circulation, slower photochemical loss and a
 374 longer lifetime of O₃ in the troposphere allowing greater transport of stratospheric O₃ to the ground.



375

376

377 Figure 7 Contributions of different sources to surface O₃ under present day and net zero conditions over
 378 East Asia (a, c) and Eastern China (b, d).

379 Over Eastern China (Figure 7b), the contribution from East Asian sources is highest, especially in
 380 summer when it exceeds 70%. Biogenic, oceanic and South Asian sources make a smaller contribution
 381 over this region, only 6%, 10%, and 3% on average, respectively. Under net zero (Figure 7d), the
 382 contribution of East Asian sources drops to 42% in summer, but remains the dominant source of surface
 383 O₃ in Eastern China. The contribution of biogenic sources is enhanced, especially in summer, reaching
 384 40%, close to the contribution from East Asian sources. The stratospheric contribution (STR) is highest
 385 in early spring (25%, 11 ppbv), and lowest in summer (2%, 1 ppbv). Under net zero, STR is enhanced to



386 40% (17 ppbv) in March and 3% (1 ppbv) in summer, similar to the seasonal contributions over East
387 Asia. In addition, the excess NO concentration in heavily urbanized Eastern China has a titration effect
388 on O₃, but the strong future decreases in NO weaken this effect, reducing the loss of stratospheric O₃ as
389 well as O₃ from local sources. Overall, surface O₃ shows substantial decreases through much of the year,
390 and the local contribution is reduced, which highlights the beneficial role that net zero policies may have
391 for controlling surface O₃ pollution in China.

392 **6 Summary and conclusions**

393 We quantify tropospheric O₃ budgets, spatiotemporal distributions of future surface O₃ in East Asia and
394 regional O₃ source contributions for 2060 under a net zero scenario, using the NCAR Community Earth
395 System Model (CESM) and online O₃ tagging methods. The simulated monthly mean global tropospheric
396 column O₃ and surface O₃ mixing ratios over East Asia capture the general features in observations well
397 under present day conditions. The offline simulations perform better than online simulations, as the
398 nudging provides a closer match to observed meteorological conditions. The tropospheric O₃ burden and
399 budget terms under present-day conditions in this study also matches those of previous model studies
400 well.

401 The simulated tropospheric O₃ burden is likely to decrease from 316 Tg under present day conditions to
402 247 Tg by 2060 under the net zero scenario. This brings it close to that found in previous studies under
403 preindustrial conditions of 239±22 Tg (Young et al., 2013). Future tropospheric O₃ chemical production
404 and loss are both reduced, and the net chemical tendency decreases from 397 to 81 Tg(O₃) yr⁻¹. The
405 contribution of stratospheric O₃ increases from 69 to 77 Tg, due to enhancement of atmospheric
406 circulation and increased stratosphere-troposphere exchange caused by climate change and the longer
407 chemical lifetime of stratospheric O₃ in the troposphere under decreased anthropogenic emissions of
408 pollutants. The mean tropospheric lifetime of O₃ is increased by 2 days, ~10%. Over East Asia, one of
409 the highest anthropogenic emissions regions, the O₃ burden decreases from 25 to 19 Tg, and the net
410 chemical tendency drops from 227 to 137 Tg(O₃) yr⁻¹. East Asia is a region of net O₃ production, and the
411 outflow is expected to decrease from 89 to 38 Tg(O₃) yr⁻¹. The burden of O₃ from the stratosphere
412 increases from 5 to 6 Tg. The lifetime of tropospheric O₃ over East Asia is shorter than the global average,
413 ~15 days, due to the high anthropogenic emissions, but increases by 2 days, similar to the global mean.
414 Compared with other SSP scenarios, particularly the much-studied SSP3-7.0 pathway, SSP1-1.9 provides
415 a more positive perspective on the opportunities for controlling future tropospheric O₃.

416 Regional average surface O₃ decreases throughout the year over East Asia, with highest decreases in
417 summer (16 ppbv) in the future under net zero scenario. Over Eastern China, the peak in surface O₃ shifts
418 from July to May. Surface O₃ decreases strongly in July (34 ppbv), and increases in winter, especially in
419 January, 12 ppbv. The increased O₃ in winter is caused by reduced titration of O₃ by NO associated with
420 lower anthropogenic NO emissions, and enhanced stratospheric input. The tropospheric O₃ over most
421 regions decreases due to the large decrease in O₃ precursors emissions. Climate change leads to only a
422 small increase in tropospheric O₃ under this scenario. Local anthropogenic emissions play a dominant
423 role in controlling O₃ changes over East Asia in summer, but this will drop substantially from 30% in



424 present day to 14% under net zero. The contribution of biogenic sources is enhanced, and forms the
425 dominant contributor to future surface O₃, especially in summer, ~40%. This enhanced contribution of
426 biogenic sources is due here to increased O₃ production efficiency associated with reduced O₃ precursors
427 concentrations, but may be underestimated if biogenic emissions also increase in future as expected. The
428 lower extent of climate change along SSP119 leads to relatively little impact on tropospheric O₃ under
429 net zero, while the emission reductions associated with net zero policies are sufficient to mitigate surface
430 O₃ pollution over East Asia, especially in summer.

431 The combined emissions and O₃ tagging method used here provide a reliable way to quantify the changes
432 of tropospheric O₃ and its sources in future under a net zero scenario. The results of this study clarify the
433 separate impacts of climate change and emissions on tropospheric O₃ changes over East Asia, and
434 highlight the significance of controlling O₃ precursors emissions along the net zero scenario, especially
435 anthropogenic emissions. The reduction of anthropogenic O₃ precursors emission should be the most
436 effective way to control the increase of tropospheric O₃, which requires joint efforts on a global scale.

437

438 **Competing interests**

439 The authors declare that they have no conflict of interest.

440 **Acknowledgements**

441 This study was supported by the National Key Research and Development Program of China (Grant No.,
442 2022YFC3701204) and the National Natural Science Foundation of China (Grant No., 42021004).
443 Numerical calculations in this paper have been performed on the high-performance computing system at
444 the High Performance Computing Center, Nanjing University of Information Science and Technology.
445 The authors would like to thank Prof. Tim Butler and Dr. Aurelia Lupascu at the Institute for Advanced
446 Sustainability Studies (now the Research Institute for Sustainability) in Potsdam, Germany for helping
447 us to update the TOAST source attribution code in the CESM model.

448 **Data availability**

449 CAQRA can be freely downloaded at <https://doi.org/10.11922/sciencedb.00053>, and the prototype
450 product, which contains the monthly and annual means of the CAQRA dataset, is available at
451 <https://doi.org/10.11922/sciencedb.00092>. The simulated O₃ data generated in this study are available
452 upon request.

453

454 **References:**

455 Akritidis, D., Pozzer, A., and Zanis, P.: On the impact of future climate change on tropopause folds and
456 tropospheric ozone, *Atmos. Chem. Phys.*, 19, 14387–14401, [https://doi.org/10.5194/acp-19-14387-](https://doi.org/10.5194/acp-19-14387-2019)
457 2019, 2019.



- 458 Bowman, H., Turnock, S., Bauer, S. E., Tsigaridis, K., Deushi, M., Oshima, N., O'Connor, F. M.,
459 Horowitz, L., Wu, T., Zhang, J., Kubistin, D., and Parrish, D. D.: Changes in anthropogenic precursor
460 emissions drive shifts in the ozone seasonal cycle throughout the northern midlatitude troposphere,
461 *Atmos. Chem. Phys.*, 22, 3507–3524, <https://doi.org/10.5194/acp-22-3507-2022>, 2022.
- 462 Butchart, N.: The Brewer-Dobson circulation, *Reviews of Geophysics*, 52(2):157-184,
463 <https://doi.org/10.1002/2013RG000448>, 2014.
- 464 Butchart, N., Charlton-Perez, A. J., Cionni, I., Hardiman, S. C., Haynes, P. H., Kruger, K., Kushner, P.
465 J., Newman, P. A., Osprey, S. M., Perlwitz, J., Sigmond, M., Wang, L., Akiyoshi, H., Austin, J.,
466 Bekki, S., Baumgaertner, A., Braesicke, P., Bruhl, C., Chipperfield, M., Dameris, M., Dhomse, S.,
467 Eyring, V., Garcia, R., Gamy, H., Jockel, P., Lamarque, J.-F., Marchand, M., Michou, M.,
468 Morgenstern, O., Nakamura, T., Pawson, S., Plummer, D., Pyle, J., Rozanov, E., Scinocca, J.,
469 Shepherd, T. G., Shibata, K., Smale, D., Teyssedre, H., Tian, W., Waugh, D. and Yamashita, Y.:
470 Multi-model climate and variability of the stratosphere, *J. Geophys. Res.*, 116, D05102,
471 <https://doi.org/10.1029/2010JD014995>, 2011.
- 472 Butler, T., Lupascu, A., Coates, J., and Zhu, S.: TOAST 1.0: Tropospheric Ozone Attribution of Sources
473 with Tagging for CESM 1.2.2, *Geosci. Model Dev.*, 11, 2825–2840, [https://doi.org/10.5194/gmd-11-](https://doi.org/10.5194/gmd-11-2825-2018)
474 [2825-2018](https://doi.org/10.5194/gmd-11-2825-2018), 2018.
- 475 Butler, T., Lupascu, A. and Nalam A.: Attribution of ground-level ozone to anthropogenic and natural
476 sources of nitrogen oxides and reactive carbon in a global chemical transport model, *Atmos. Chem.*
477 *Phys.*, 20, 10707–10731, <https://doi.org/10.5194/acp-20-10707-2020>, 2020.
- 478 Cheng, J., Tong, D., Zhang, Q., Liu, Y., Lei, Y., Yan, G., Yan, L., Yu, S., Cui, R. Y., Clarke, L., Geng,
479 G. N., Zheng, B., Zhang, X. Y., Davis, J. S., and He, K. B.: Pathways of China's PM_{2.5} air quality
480 2015–2060 in the context of carbon neutrality, *Natl. Sci. Rev.*, nwab078,
481 <https://doi.org/10.1093/nsr/nwab078>, 2021.
- 482 Cionni, I., Eyring, V., Lamarque, J.F., Randel, W.J., Stevenson, D.S., Wu, F., Bodeker, G.E., Shepherd,
483 T.G., Shindell, D.T., Waugh, D.W.: Ozone database in support of CMIP5 simulations: results and
484 corresponding radiative forcing, *Atmos. Chem. Phys.*, 11, 11267–11292. [https://doi.org/10.5194/acp-](https://doi.org/10.5194/acp-11-11267-2011)
485 [11-11267-2011](https://doi.org/10.5194/acp-11-11267-2011), 2011.
- 486 Danabasoglu, G., Lamarque, J. -F., Bacmeister, J., Bailey, D. A., DuVivier, A. K., Edwards, J., Emmons,
487 L. K., Fasullo, J., Garcia, R., Gettelman, A., Hannay, C., Holland, M. M., Large, W. G., Lauritzen, P.
488 H., Lawrence, D. M., Lenaerts, J. T. M., Lindsay, K., Lipscomb, W. H., Mills, M. J., Neale, R., Oleson,
489 K. W., Otto-Bliesner, B., Phillips, A. S., Sacks, W., Tilmes, S., Kampenhou, L. van, Vertenstein, M.,
490 Bertini, A., Dennis, J., Deser, C., Fischer, C., Fox-Kemper, B., Kay, J. E., Kinnison, D., Kushner, P.
491 J., Larson, V. E., Long, M. C., Mickelson, S., Moore, J. K., Nienhouse, E., Polvani, L., Rasch, P. J.,
492 Strand, W. G.: The Community Earth System Model Version 2 (CESM2), *J. Adv. Model. Earth Syst.*,
493 12(2). <https://doi.org/10.1029/2019MS001916>, 2020.



- 494 Emberson, L.: Effects of ozone on agriculture, forests and grasslands, *Philosophical Transactions of The*
495 *Royal Society A Mathematical Physical and Engineering Sciences*, 378(2183):20190327,
496 <https://doi.org/10.1098/rsta.2019.0327>, 2020.
- 497 Emmons, L. K., Walters, S., Hess, P. G., Lamarque, J.-F., Pfister, G. G., Fillmore, D., Granier, C.,
498 Guenther, A., Kinnison, D., Laepple, T., Orlando, J., Tie, X., Tyndall, G., Wiedinmyer, C., Baughcum,
499 S. L., and Kloster, S.: Description and evaluation of the Model for Ozone and Related chemical
500 Tracers, version 4 (MOZART-4), *Geosci. Model Dev.*, 3, 43–67, [https://doi.org/10.5194/gmd-3-43-](https://doi.org/10.5194/gmd-3-43-2010)
501 2010, 2010.
- 502 Griffiths, P. T., Murray, L. T., Zeng, G., Shin, Y. M., Abraham, N. L., Archibald, A. T., Deushi, M.,
503 Emmons, L. K., Galbally, I. E., Hassler, B., Horowitz, L. W., Keeble, J., Liu, J., Moeini, O., Naik,
504 V., O'Connor, F. M., Oshima, N., Tarasick, D., Tilmes, S., Turnock, S. T., Wild, O., Young, P. J.,
505 and Zanis, P.: Tropospheric ozone in CMIP6 simulations, *Atmos. Chem. Phys.*, 21, 4187–4218,
506 <https://doi.org/10.5194/acp-21-4187-2021>, 2021.
- 507 Guenther, A. B., Jiang, X., Heald, C. L., Sakulyanontvittaya, T., Duhl, T., Emmons, L. K., and Wang,
508 X.: The Model of Emissions of Gases and Aerosols from Nature version 2.1 (MEGAN2.1): An
509 extended and updated framework for modeling biogenic emissions, *Geosci. Model Dev.*, 5(6), 1471–
510 1492, <https://doi.org/10.5194/gmd-5-1471-2012>, 2012.
- 511 Guenther, A., Karl, T., Harley, P., Wiedinmyer, C., Palmer, P. I., and Geron, C.: Estimates of global
512 terrestrial isoprene emissions using MEGAN (Model of Emissions of Gases and Aerosols from
513 Nature), *Atmos. Chem. Phys.*, 6, 3181–3210, [https://doi.org/10.5194/acp-6-](https://doi.org/10.5194/acp-6-3181-2006) 3181-2006, 2006.
- 514 Heald, C. L., Henze, D. K., Horowitz, L. W., Feddema, J., Lamarque, J.-F., Guenther, A., Hess, P. G.,
515 Vitt, F., Seinfeld, J. H., Goldstein, A. H., and Fung, I.: Predicted change in global secondary organic
516 aerosol concentrations in response to future climate, emissions, and land use change, *J. Geophys.*
517 *Res.-Atmos.*, 113, D05211, <https://doi.org/10.1029/2007JD009092>, 2008.
- 518 Hong, C. P., Zhang, Q., Zhang, Y., Davis, S. J., Tong, D., Zheng, Y. X., Liu, Z., Guan, D., He, K. B.,
519 Schellnhuber, H. J.: Impacts of climate change on future air quality and human health in China, *Proc*
520 *Natl Acad Sci*, 116(35), 17193–17200, <https://doi.org/10.1073/pnas.1812881116>, 2019.
- 521 Janssens-Maenhout, G., Crippa, M., Guizzardi, D., Dentener, F., Muntean, M., Pouliot, G., Keating, T.,
522 Zhang, Q., Kurokawa, J., Wankmüller, R., Denier van der Gon, H., Kuenen, J. J. P., Klimont, Z.,
523 Frost, G., Darras, S., Koffi, B., and Li, M.: HTAP_v2.2: a mosaic of regional and global emission
524 grid maps for 2008 and 2010 to study hemispheric transport of air pollution, *Atmos. Chem. Phys.*, 15,
525 11411–11432, <https://doi.org/10.5194/acp-15-11411-2015>, 2015.
- 526 Jerrett, M., Burnett, R.T., Pope, C.A., Ito, K., Thurston, G., Krewski, D., Shi, Y., Calle, E., Thun, M.:
527 Long-term ozone exposure and mortality, *N. Engl. J. Med.*, 360, 1085–1095.
528 <https://doi.org/10.1056/NEJMoa0803894>, 2009.



- 529 Kawase, H., Nagashima, T., Sudo, K., Nozawa, T.: Future changes in tropospheric ozone under
530 representative concentration pathways (RCPs), *Geophys. Res. Lett.* 38, L05801.
531 <https://doi.org/10.1029/2010GL046402>, 2011.
- 532 Karset, I. H. H., Berntsen, T. K., Storelvmo, T., Alterskjær, K., Grini, A., Olivié, D., Kirkevåg, A., Seland,
533 Ø., Iversen, T., and Schulz, M.: Strong impacts on aerosol indirect effects from historical oxidant
534 changes, *Atmos. Chem. Phys.*, 18, 7669–7690, <https://doi.org/10.5194/acp-18-7669-2018>, 2018.
- 535 Kim, M.J., Park, R.J., Ho, C.-H., Woo, J.-H., Choi, K.-C., Song, C.-K., Lee, J.-B.: Future ozone and
536 oxidants change under the RCP scenarios, *Atmos. Environ.* 101, 103–115.
537 <https://doi.org/10.1016/J.ATMOSENV.2014.11.016>, 2015.
- 538 Kinnison, D. E., Brasseur, G. P., Walters, S., Garcia, R. R., Marsch, D. A., Sassi, F., Boville, B. A.,
539 Harvey, V. L., Randall, C. E., Emmons, L., Lamarque, J. F., Hess, P., Orlando, J. J., Tie, X. X.,
540 Randel, W., Pan, L. L., Gettelman, A., Granier, C., Diehl, T., Niemaier, U., and Simmons, A. J.:
541 Sensitivity of chemical tracers to meteorological parameters in the MOZART-3 chemical transport
542 model, *J. Geophys. Res.*, 112, D20302, <https://doi.org/10.1029/2006JD007879>, 2007.
- 543 Kleinman, I., Daum, P. H., Lee, Y.-N., Nunnermacker, L. J., Springston, S. R., Weinstein-Lloyd, J.,
544 Rudolph, J.: Ozone production efficiency in an urban area, *J. Geophys. Res.*, 107(D23):4733,
545 <https://doi.org/10.1029/2002JD002529>, 2002.
- 546 Koffi, B., Dentener, F., Janssens-Maenhout, G., Guizzardi, D., Crippa, M., Diehl, T., Galmarini, S.,
547 Solazzo, E.: Hemispheric Transport Air Pollution (HTAP): Specification of the HTAP2 experiments–
548 Ensuring harmonized modelling, EUR 28255 EN, Luxembourg: Publications Office of the European
549 Union, <https://doi.org/10.2788/725244>, 2016.
- 550 Kong, L., Tang, X., Zhu, J., Wang, Z., Li, J., Wu, H., Wu, Q., Chen, H., Zhu, L., Wang, W., Liu, B.,
551 Wang, Q., Chen, D., Pan, Y., Song, T., Li, F., Zheng, H., Jia, G., Lu, M., Wu, L., and Carmichael, G.
552 R.: A 6-year-long (2013–2018) high-resolution air quality reanalysis dataset in China based on the
553 assimilation of surface observations from CNEMC, *Earth Syst. Sci. Data*, 13, 529–570,
554 <https://doi.org/10.5194/essd-13-529-2021>, 2021.
- 555 Lamarque, J.-F., Emmons, L. K., Hess, P. G., Kinnison, D. E., Tilmes, S., Vitt, F., Heald, C. L., Holland,
556 E. A., Lauritzen, P. H., Neu, J., Orlando, J. J., Rasch, P. J., and Tyndall, G. K.: CAM-chem:
557 description and evaluation of interactive atmospheric chemistry in the Community Earth System
558 Model, *Geosci. Model Dev.*, 5, 369–411, <https://doi.org/10.5194/gmd-5-369-2012>, 2012.
- 559 Lamarque, J.-F., Shindell, D.T., Josse, B., Young, P.J., Cionni, I., Eyring, V., Bergmann, D., Cameron-
560 Smith, P., Collins, W.J., Doherty, R., Dalsoren, S., Faluvegi, G., Folberth, G., Ghan, S.J., Horowitz,
561 L.W., Lee, Y.H., MacKenzie, I.A., Nagashima, T., Naik, V., Plummer, D., Righi, M., Rumbold, S.T.,
562 Schulz, M., Skeie, R.B., Stevenson, D.S., Strode, S., Sudo, K., Szopa, S., Voulgarakis, A., Zeng, G.:
563 The Atmospheric Chemistry and Climate Model Intercomparison Project (ACCMIP): overview and



- 564 de- scription of models, simulations and climate diagnostics, *Geosci. Model Dev.*, 6, 179–206,
565 <https://doi.org/10.5194/gmd-6-179-2013>, 2013.
- 566 Li, J., Nagashima, T., Kong, L., Ge, B., Yamaji, K., Fu, J. S., Wang, X., Fan, Q., Itahashi, S., Lee, H.-J.,
567 Kim, C.-H., Lin, C.-Y., Zhang, M., Tao, Z., Kajino, M., Liao, H., Li, M., Woo, J.-H., Kurokawa, J.,
568 Wang, Z., Wu, Q., Akimoto, H., Carmichael, G. R., and Wang, Z.: Model evaluation and
569 intercomparison of surface-level ozone and relevant species in East Asia in the context of MICS-Asia
570 Phase III – Part 1: Overview, *Atmos. Chem. Phys.*, 19, 12993–13015, <https://doi.org/10.5194/acp-19-12993-2019>, 2019.
- 572 Liu, G., Liu, J. J., Tarasick, D. W., Fioletov, V. E., Liu, J., Jin, J., Moeini, O., Sioris, C. E. and Osman,
573 M.: A global tropospheric ozone climatology from trajectory-mapped ozone soundings, *Atmos. Chem.*
574 *Phys.* 13, 10659-10675, <https://doi.org/10.5194/acp-13-10659-2013>, 2013.
- 575 Liu, J., Tarasick, D. W., Fioletov, V. E., McLinden C., Zhao, T., Gong, S., Sioris, C., Jin, J., Liu, G., and
576 Moeini, O.: A Global Ozone Climatology from Ozone Soundings via Trajectory Mapping: A
577 Stratospheric Perspective, *Atmos. Chem. Phys.*, 13, 11441-11464, <https://doi.org/10.5194/acp-13-11441-2013>, 2013.
- 579 Liu, Z., Doherty, R. M., Wild, O., O'Connor, F. M., and Turnock, S. T.: Tropospheric ozone changes and
580 ozone sensitivity from the present day to the future under shared socio-economic pathways, *Atmos.*
581 *Chem. Phys.*, 22, 1209–1227, <https://doi.org/10.5194/acp-22-1209-2022>, 2022.
- 582 Lu, X., Zhang, L., and Shen, L.: Meteorology and Climate Influences on Tropospheric Ozone: a Review
583 of Natural Sources, Chemistry, and Transport Patterns, *Current Pollution Reports*, 5:238–260,
584 <https://doi.org/10.1007/s40726-019-00118-3>, 2019.
- 585 Lu, X., Zhang, L., Wang, X., Gao, M., Li, K., Zhang, Y., Yue, X., and Zhang, Y.: Rapid Increases in
586 Warm-Season Surface Ozone and Resulting Health Impact in China since 2013, *Environ. Sci.*
587 *Technol. Lett.*, 7, 240–247, <https://doi.org/10.1021/acs.estlett.0c00171>, 2020.
- 588 Malley, C. S., Henze, D. K., Kuylentierna, J. C. I., Vallack, H. W., Davila, Y., Anenberg, S. C., Turner,
589 M. C., Ashmore, M. R.: Updated global estimates of respiratory mortality in adults ≥ 30 Years of age
590 attributable to long-term ozone exposure, *Environ. Health Perspect*, 125, 87021,
591 <https://doi.org/10.1289/EHP1390>, 2017.
- 592 Myhre, G., Shindell, D., Breon, F.-M., Collins, W., Fuglestedt, J., Huang, J., Koch, D., Lamarque, J.-
593 F., Lee, D., Mendoza, B., Nakajima, T., Robock, A., Stephens, G., Takemura, T., Zhang, H.:
594 Anthropogenic and natural radiative forcing. In: *Climate Change 2013: the Physical Science Basis.*
595 Contribution of Working Group I to the Fifth Assessment Report of the Intergovernmental Panel on
596 Climate Change. Cambridge University Press, Cambridge, United Kingdom and New York, NY,
597 USA, 659-740, 2013.



- 598 Neale, R. B., Richter, J., Park, S., Lauritzen, P. H., Vavrus, S. J., Rasch, P. J., and Zhang, M.: The Mean
599 Climate of the Community Atmosphere Model (CAM4) in forced SST and fully coupled experiments,
600 *J. Climate*, 26, 5150–5168, <https://doi.org/10.1175/JCLI-D-12-00236.1>, 2013.
- 601 O'Connor, F. M., Johnson, C. E., Morgenstern, O., Abraham, N. L., Braesicke, P., Dalvi, M., Folberth,
602 G. A., Sanderson, M. G., Telford, P. J., Voulgarakis, A., Young, P. J., Zeng, G., Collins, W. J., Pyle,
603 J. A.: Evaluation of the new UKCA climate-composition model – Part 2: the Troposphere, *Geosci.*
604 *Model Dev.*, 7, 41–91, <https://doi.org/10.5194/gmd-7-41-2014>, 2014.
- 605 Oleson, K. W., Lawrence, D. M., Bonan, G. B., Flanner, M. G., Kluzek, E., Lawrence, P. J., Levis, S.,
606 Sean C. Swenson, S. C., Peter, E. T., Dai, A., Decker, M., Dickinson, R., Feddema, J., Heald, C. L.,
607 Hoffman, F., Lamarque, J.-F., Mahowald, N., Niu, G.-Y., Qian, T., Randerson, J., Running, S.,
608 Sakaguchi, K., Slater, A., Stöckli, R., Wang, A., Yang, Z. L., Zeng, X.: Technical Description of
609 version 4.0 of the Community Land Model (CLM) (No. NCAR/TN-478+STR), University
610 Corporation for Atmospheric Research. <http://dx.doi.org/10.5065/D6FB50WZ>, 2010.
- 611 O'Neill, B. C., Krieglner, E., Riahi, K., Ebi, K. L., Hallegatte, S., Carter, T. R., Mathur, R., van Vuuren,
612 D. P.: A new scenario framework for climate change research: the concept of shared socioeconomic
613 pathways, *Clim. Change*, 122, 387–400, <https://doi.org/10.1007/s10584-013-0905-2>, 2014.
- 614 Rao, S., Klimont, Z., Smith, S.J., Dingenen, R. Van, Dentener, F., Bouwman, L., Riahi, K., Amann, M.,
615 Bodirsky, B.L., Van Vuuren, D.P., Reis, L.A., Calvin, K., Drouet, L., Fricko, O., Fujimori, S.,
616 Gernaat, D., Havlik, P., Harmsen, M., Hasegawa, T., Heyes, C., Hilaire, J., Luderer, G., Masui, T.,
617 Stehfest, E., Strefler, J., Van Der Sluis, S., Tavoni, M.: Future air pollution in the shared socio-
618 economic pathways, *Glob. Environ. Chang.*, 42, 346–358,
619 <https://doi.org/10.1016/j.gloenvcha.2016.05.012>, 2017.
- 620 Riahi, K., Van Vuuren, D.P., Krieglner, E., Edmonds, J., O'Neill, B.C., Fujimori, S., Bauer, N., Calvin,
621 K., Dellink, R., Fricko, O., Lutz, W., Popp, A., Cuaresma, J.C., Kc, S., Leimbach, M., Jiang, L., Kram,
622 T., Rao, S., Emmerling, J., Ebi, K., Hasegawa, T., Havlik, P., Humpenöder, F., Aleluia, L., Silva, D.,
623 Smith, S., Stehfest, E., Bosetti, V., Eom, J., Gernaat, D., Masui, T., Rogelj, J., Strefler, J., Drouet, L.,
624 Krey, V., Luderer, G., Harmsen, M., Takahashi, K., Baumstark, L., Doelman, J.C., Kainuma, M.,
625 Klimont, Z., Marangoni, G., Lotze-Campen, H., Obersteiner, M., Tabeau, A., Tavoni, M.: The Shared
626 Socioeconomic Pathways and their energy, land use, and greenhouse gas emissions implications: an
627 overview, *Glob. Environ. Chang.*, 42, 153–168, <https://doi.org/10.1016/j.gloenvcha.2016.05.009>,
628 2017.
- 629 Rienecker, M. M., Suarez, M. J., Gelaro, R., Todling, R., Bacmeister, J., Liu, E., Bosilovich, M. G.,
630 Schubert, S. D., Takacs, L., Kim, G.-K., Bloom, S., Chen, J., Collins, D., Conaty, A., da Silva, A.,
631 Gu, W., Joiner, J., Koster, R. D., Lucchesi, R., Molod, A., Owens, T., Pawson, S., Pegion, P., Redder,
632 C. R., Reichle, R., Robertson, F. R., Ruddick, A. G., Sienkiewicz, M., and Woollen, J.: MERRA:
633 NASA's Modern-Era Retrospective Analysis for Research and Application, *J. Climate*, 24, 3624–
634 3648, <https://doi.org/10.1175/JCLI-D-11-00015.1>, 2011.



- 635 Sander, S. P., Friedl, R. R., Barker, J. R., Golden, D. M., Kurylo, M. J., Sciences, G. E., Wine, P. H.,
636 Abbatt, J. P. D., Burkholder, J. B., Kolb, C. E., Moortgat, G. K., Huie, R. E., and Orkin, V. L.:
637 Chemical Kinetics and Photochemical Data for Use in Atmospheric Studies Evaluation Number 17
638 NASA Panel for Data Evaluation, JLP Publ., 10–6, 2011.
- 639 Shi, X., Zheng, Y., Lei, Y., Xue, W., Yan, G., Liu, X., Cai, B., Tong, D., Wang, J.: Air quality benefits
640 of achieving carbon neutrality in China, *Sci. Total Environ.*, 795, 148784,
641 <https://doi.org/10.1016/j.scitotenv.2021.148784>, 2021.
- 642 Shindell, D. T., Faluvegi, G., Koch, D. M., Schmidt, G. A., Unger, N., and Bauer, S. E.: Improved
643 Attribution of Climate Forcing to Emissions, *Science*, 326, 716–718,
644 <https://doi.org/10.1126/science.1174760>, 2009.
- 645 Stevenson, D. S., Dentener, F. J., Schultz, M. G., Ellingsen, K., van Noije, T. P. C., Wild, O., Zeng, G.,
646 Amann, M., Atherton, C. S., Bell, N., Bergmann, D. J., Bey, I., Butler, T., Cofala, J., Collins, W. J.,
647 Derwent, R. G., Doherty, R. M., Drevet, J., Eskes, H. J., Fiore, A. M., Gauss, M., Hauglustaine, D.
648 A., Horowitz, L. W., Isaksen, I. S. A., Krol, M. C., Lamarque, J.-F., Lawrence, M. G., Montanaro,
649 V., Müller, J.-F., Pitari, G., Prather, M. J., Pyle, J. A., Rast, S., Rodriguez, J. M., Sanderson, M. G.,
650 Savage, N. H., Shindell, D. T., Strahan, S. E., Sudo, K., Szopa, S.: Multi-model ensemble simulations
651 of present-day and near future tropospheric ozone, *J. Geophys. Res.*, 111, D08301,
652 <https://doi.org/10.1029/2005JD006338>, 2006.
- 653 Stevenson, D. S., Young, P. J., Naik, V., Lamarque, J.-F., Shindell, D. T., Voulgarakis, A., Skeie, R. B.,
654 Dalsoren, S. B., Myhre, G., Berntsen, T. K., Folberth, G. A., Rumbold, S. T., Collins, W. J.,
655 MacKenzie, I. A., Doherty, R. M., Zeng, G., van Noije, T. P. C., Strunk, A., Bergmann, D., Cameron-
656 Smith, P., Plummer, D. A., Strode, S. A., Horowitz, L., Lee, Y. H., Szopa, S., Sudo, K., Nagashima,
657 T., Josse, B., Cionni, I., Righi, M., Eyring, V., Conley, A., Bowman, K. W., Wild, O., Archibald, A.:
658 Tropospheric ozone changes, radiative forcing and attribution to emissions in the atmospheric
659 chemistry and climate model Intercomparison project (ACCMIP), *Atmos. Chem. Phys.* 13, 3063–
660 3085. <https://doi.org/10.5194/acp-13-3063-2013>, 2013.
- 661 Sudo, K., Takahashi, M., and Akimoto, H.: Future changes in stratosphere-troposphere exchange and
662 their impacts on future tropospheric ozone simulations, *Geophys. Res. Lett.*, 30(24), 2256,
663 <https://doi.org/10.1029/2003GL018526>, 2003.
- 664 Tang, X., Zhu, J., Wang, Z. F., and Gbaguidi, A.: Improvement of ozone forecast over Beijing based on
665 ensemble Kalman filter with simultaneous adjustment of initial conditions and emissions, *Atmos.*
666 *Chem. Phys.*, 11, 12901–12916, <https://doi.org/10.5194/acp-11-12901-2011>, 2011.
- 667 Tang, X., Kong, L., Zhu, J., Wang, Z. F., Li, J. J., Wu, H. J., Wu, Q. Z., Chen, H. S., Zhu, L. L., Wang,
668 W., Liu, B., Wang, Q., Chen D. H., Pan Y. P., Song, T., Li, F., Zheng, H. T., Jia, G. L., Lu, M. M.,
669 Wu, L., and Carmichael, G. R.: A Six-year long High-resolution Air Quality Reanalysis Dataset over
670 China from 2013 to 2018, V2, *Sci. Data Bank*, <https://doi.org/10.11922/sciencedb.00053>, 2020a.



- 671 Tang, X., Kong, L., Zhu, J., Wang, Z. F., Li, J. J., Wu, H. J., Wu, Q. Z., Chen, H. S., Zhu, L. L., Wang,
672 W., Liu, B., Wang, Q., Chen D. H., Pan Y. P., Song, T., Li, F., Zheng, H. T., Jia, G. L., Lu, M. M.,
673 Wu, L., and Carmichael, G. R.: A Six-year long High-resolution Air Quality Reanalysis Dataset over
674 China from 2013 to 2018 (monthly and annual version), V1, Sci. Data Bank,
675 <https://doi.org/10.11922/sciencedb.00092>, 2020b.
- 676 Tie, X., Madronich, S., Walters, S., Edwards, D. P., Ginoux, P., Mahowald, N., Zhang, R. Y., Lou, C.,
677 Brasseur, G.: Assessment of the global impact of aerosols on tropospheric oxidants, *J. Geophys. Res.*,
678 110, D03204, <https://doi.org/10.1029/2004JD005359>, 2005.
- 679 Tilmes, S., Lamarque, J.-F., Emmons, L. K., Kinnison, D. E., Ma, P.-L., Liu, X., Ghan, S., Bardeen, C.,
680 Arnold, S., Deeter, M., Vitt, F., Ryerson, T., Elkins, J. W., Moore, F., Spackman, J. R., and Val
681 Martin, M.: Description and evaluation of tropospheric chemistry and aerosols in the Community
682 Earth System Model (CESM1.2), *Geosci. Model Dev.*, 8, 1395–1426, [https://doi.org/10.5194/gmd-](https://doi.org/10.5194/gmd-8-1395-2015)
683 8-1395-2015, 2015.
- 684 Tong, D., Cheng, J., Liu, Y., Yu, S., Yan, L., Hong, C., Qin, Y., Zhao, H., Zheng, Y., Geng, G., Li, M.,
685 Liu, F., Zhang, Y., Zheng, B., Clarke, L., and Zhang, Q.: Dynamic projection of anthropogenic
686 emissions in China: methodology and 2015–2050 emission pathways under a range of socio-
687 economic, climate policy, and pollution control scenarios, *Atmos. Chem. Phys.*, 20, 5729–5757,
688 <https://doi.org/10.5194/acp-20-5729-2020>, 2020.
- 689 Turnock, S. T., Wild, O., Sellara, A., O'Connor, F. M.: 300 years of tropospheric ozone changes using
690 CMIP6 scenarios with a parameterised approach. *Atmos. Environ.*, 213, 686–698,
691 <https://doi.org/10.1016/j.atmosenv.2019.07.001>, 2019.
- 692 Turnock, S. T., Wild, O., Dentener, F. J., Davila, Y., Emmons, L. K., Flemming, J., Folberth, G. A.,
693 Henze, D. K., Jonson, J. E., Keating, T. J., Kengo, S., Lin, M., Lund, M., Tilmes, S., O'Connor, F.
694 M.: The impact of future emission policies on tropospheric ozone using a parameterised approach,
695 *Atmos. Chem. Phys.* 18, 8953–8978, <https://doi.org/10.5194/acp-18-8953-2018>, 2018.
- 696 Voulgarakis, A., Naik, V., Lamarque, J.-F., Shindell, D. T., Young, P. J., Prather, M. J., Wild, O., Field,
697 R. D., Bergmann, D., CameronSmith, P., Cionni, I., Collins, W. J., Dalsøren, S. B., Doherty, R. M.,
698 Eyring, V., Faluvegi, G., Folberth, G. A., Horowitz, L. W., Josse, B., MacKenzie, I. A., Nagashima,
699 T., Plummer, D. A., Righi, M., Rumbold, S. T., Stevenson, D. S., Strode, S. A., Sudo, K., Szopa, S.,
700 and Zeng, G.: Analysis of present day and future OH and methane lifetime in the ACCMIP
701 simulations, *Atmos. Chem. Phys.*, 13, 2563–2587, <https://doi.org/10.5194/acp-13-2563-2013>, 2013.
- 702 Wang, Y., Liao, H.: The impacts of transport from South and Southeast Asia on O₃ concentrations in
703 China from 2015 to 2050, *Chinese Science Bulletin (in Chinese)*, 67(18), 2043–2059,
704 <https://doi.org/10.1360/tb-2021-0707>, 2022.



- 705 Wang Y., Shen, L., Wu, S., Mickley, L., He, J., Hao, J.: Sensitivity of surface ozone over China to 2000–
706 2050 global changes of climate and emissions, *Atmos. Environ.*, 75, 374–382,
707 <https://doi.org/10.1016/j.atmosenv.2013.04.045>, 2013.
- 708 Wang, T., Wei, X. L., Ding, A. J., Poon, C. N., Lam, K. S., Li, Y. S., Chan, L. Y., and Anson, M.:
709 Increasing surface ozone concentrations in the background atmosphere of Southern China, 1994–
710 2007, *Atmos. Chem. Phys.*, 9, 6217–6227, <https://doi.org/10.5194/acp-9-6217-2009>, 2009.
- 711 Wang, Z. F., Sha, W. M., and Ueda, H.: Numerical modeling of pollutant transport and chemistry during
712 a high-ozone event in northern Taiwan, *Tellus B*, 52, 1189–1205, <https://doi.org/10.1034/j.1600-0889.2000.01064.x>, 2000.
- 714 Wild, O.: Modelling the global tropospheric ozone budget: exploring the variability in current models,
715 *Atmos. Chem. Phys.*, 7, 2643–2660, <https://doi.org/10.5194/acp-7-2643-2007>, 2007.
- 716 Wild, O. and Akimoto, H.: Intercontinental transport of ozone and its precursors in a three-dimensional
717 global CTM, *J. Geophys. Res.*, 106(D21): 27729–27744, <https://doi.org/10.1029/2000jd000123>, 2001.
- 718 Wild, O., Fiore, A. M., Shindell, D. T., Doherty, R. M., Collins, W. J., Dentener, F. J., Schultz, M. G.,
719 Gong, S., MacKenzie, I. A., Zeng, G., Hess, P., Duncan, B. N., Bergmann, D. J., Szopa, S., Jonson,
720 J. E., Keating, T. J., and Zuber, A.: Modelling future changes in surface ozone: a parameterized
721 approach, *Atmos. Chem. Phys.*, 12, 2037–2054, <https://doi.org/10.5194/acp-12-2037-2012>, 2012.
- 722 Xu, B., Wang, T., Ma, D., Song, R., Zhang, M., Gao, L., Li, S., Zhuang, B., Li, M., Xie, M.: Impacts of
723 regional emission reduction and global climate change on air quality and temperature to attain carbon
724 neutrality in China. *Atmos. Res.*, <https://doi.org/10.1016/j.atmosres.2022.106384>, 2022.
- 725 Young, P. J., Archibald, A. T., Bowman, K. W., Lamarque, J.-F., Naik, V., Stevenson, D. S., Tilmes, S.,
726 Voulgarakis, A., Wild, O., Bergmann, D., Cameron-Smith, P., Cionni, I., Collins, W. J., Dalsøren, S.
727 B., Doherty, R. M., Eyring, V., Faluvegi, G., Horowitz, L. W., Josse, B., Lee, Y. H., MacKenzie, I.
728 A., Nagashima, T., Plummer, D. A., Righi, M., Rumbold, S. T., Skeie, R. B., Shindell, D. T., Strode,
729 S. A., Sudo, K., Szopa, S., and Zeng, G.: Pre-industrial to end 21st century projections of tropospheric
730 ozone from the Atmospheric Chemistry and Climate Model Intercomparison Project (ACCMIP),
731 *Atmos. Chem. Phys.*, 13, 2063–2090, <https://doi.org/10.5194/acp-13-2063-2013>, 2013.
- 732 Young, P. J., Naik, V., Fiore, A. M., Gaudel, A., Guo, J., Lin, M. Y., Neu, J. L., Parrish, D. D., Rieder,
733 H. E., Schnell, J. L., Tilmes, S., Wild, O., Zhang, L., Ziemke, J., Brandt, J., Delcloo, A., Doherty, R.
734 M., Geels, C., Hegglin, M. I., Hu, L., Im, U., Kumar, R., Luhar, A., Murray, L., Plummer, D.,
735 Rodriguez, J., Saiz-Lopez, A., Schultz, M. G., Woodhouse, M. T., Zeng, G.: Tropospheric Ozone
736 Assessment Report: Assessment of global-scale model performance for global and regional ozone
737 distributions, variability, and trends, *Elem. Sci. Anth.*, 2018; 6:10,
738 <https://doi.org/10.1525/elementa.265>, 2018.



- 739 Zaveri, R. A., Berkowitz, C. M., Kleinman, L. I., Springston, S. R., Doskey, P. V., Lonneman, W. A.,
740 Spicer, C. W.: Ozone production efficiency and NO_x depletion in an urban plume: Interpretation of
741 field observations and implications for evaluating O₃-NO_x-VOC sensitivity, *J. Geophys. Res.*,
742 108(D14):4436, <https://doi.org/10.1029/2002JD003144>, 2003.
- 743 Ziemke, J. R., Chandra, S., Labow, G. J., Bhartia, P. K., Froidevaux, L., and Witte, J. C.: A global
744 climatology of tropospheric and stratospheric ozone derived from Aura OMI and MLS measurements,
745 *Atmos. Chem. Phys.*, 11, 9237–9251, <https://doi.org/10.5194/acp-11-9237-2011>, 2011.
- 746 Zhu, J. and Liao, H.: Future ozone air quality and radiative forcing over China owing to future changes
747 in emissions under the Representative Concentration Pathways (RCPs), *J. Geophys. Res.: Atmos.*,
748 121: 1978 – 2001, <https://doi.org/10.1002/2015JD023926>, 2016.